IEEE Access
Multidisciplinary ⋮ Rapid Review ⋮ Open Access Journal

Received 24 January 2023, accepted 7 February 2023, date of publication 14 February 2023, date of current version 23 February 2023.

Digital Object Identifier 10.1109/ACCESS.2023.3245328

RESEARCH ARTICLE

Emission Test Method for Source Stirred Reverberation Chambers With Scalar Measurements

ALFREDO DE LEO, (Member, IEEE), PAOLA RUSSO, (Member, IEEE), AND VALTER MARIANI PRIMIANI, (Senior Member, IEEE)
Department of Information Engineering, Università Politecnica delle Marche, 60131 Ancona, Italy
Corresponding author: Alfredo De Leo (a.deleo@univpm.it)

ABSTRACT This paper describes a novel method to reconstruct the radiated emission of a device under test placed in a reverberation chamber equipped with multiple monopole source stirring technique. The method is based on the measurement of the normal component of the electric field, collected close to the walls of the chamber by the monopole antennas. The main improvement from the previous formulation of the method is that the only knowledge of the amplitude of the electric field is sufficient to reconstruct, within a predictable range of uncertainty, the maximum level of the radiation of the device over all the directions at a given distance. The consequent advantage is that the method is immediately usable in a realistic scenario for emission tests, where an EMI receiver or a spectrum analyzer are used to measure the electric field and therefore only the amplitude of the field is retrieved.

INDEX TERMS Emission test, reverberation chamber, source stirring.

I. INTRODUCTION

The reference test environment for assessing the radiated emission compliance of an equipment under test (EUT) is the open air test site (OATS). Due to many practical reasons that make almost impossible to use OATSs, other alternative test sites were developed and standardized: anechoic chambers, transverse electromagnetic cell (TEM) cells, Gigahertz transverse electromagnetic cell (GTEM) cells and reverberation chambers [1], [2], [3].

Inside a reverberation chamber (RC), radiated emissions are indirectly determined from the measurement of the total average power radiated by the EUT and the estimation of its directivity from its dimensions [4], [5], [6].

The electromagnetic field inside an RC is typically mechanically stirred by using rotating paddles [7] or moving walls [8], [9].

Another way to stir the electromagnetic field is to vary the properties of the source [10], changing the transmitting frequency, phase, or position. A wide description of RC methodologies and stirring methods can be found in [11] together with a wide literature recall. In [12] a list of the principal RC performance indicators can be found.

One particular implementation of source stirring action is the multiple monopole source stirring technique (MMSS) [13]: it is based on an array of antennas, placed onto the walls of the cavity and subsequently fed. This stirring technique has two main advantages with respect to mechanical stirring actions: the first one is that nothing is in movement inside the RC; the second one is that the effectiveness of this technique is good also at low frequency range [14], where the scattering elements become small in terms of wavelength. The main drawback is the need of an electronic switch to automatize the process.

The presence of an array of antennas, used as source for immunity test in a MMSS RC [15], [16], led the research activity to develop a method for measuring the EUT radiated emissions using the same array placed onto the RC's walls. Unlike the standard procedure of radiated emission measurement performed in a RC [4], we need no estimation of the directivity of the EUT.

The associate editor coordinating the review of this manuscript and approving it for publication was Bo Pu.

The method is based on a set of equivalent sources, properly set in the working volume of the RC. Their values are fixed to reconstruct the electric field samples collected by the antennas when the EUT is placed in the RC. To get the maximum value of radiated electric field in free space conditions, the equivalent sources' radiation is analytically computed and thus directly compared with the electric field limits provided by standards.

The method was theorized [14], [15] and experimentally validated [16] in the case we know complex values of the electric field samples.

However, in a realistic scenario, the phase information is missing. In fact, an EMI receiver or a spectrum analyzer, that are usually used for radiated emission measurements, returns only the magnitude of the electric field. The aim of this work is therefore to extend the method to the work case where it is available only the amplitude of the electric field values collected by the antennas placed onto the RC's walls.

The paper is organized as follows: section II describes the algorithm to reconstruct the radiated emission of an EUT using the electric field samples; section III shows that the radiated emission measured in RC using the proposed method are in accordance with measurements in an anechoic environment; section IV is dedicated to the study of the uncertainty; finally, conclusions are provided.

II. ALGORITHM DESCRIPTION

The algorithm to reconstruct the radiated emission from the values of electric field samples [17], [18] is here recalled for sake of completeness. It is an iterative algorithm whose steps are:

1. The EUT is placed into the working volume of the RC and the N_s monopoles, placed on the RC walls, measure the electric field ($E_i^{meas} i = 1, \ldots, N_s$).
2. A simulation phase follows: the EUT is replaced by a set of equivalent sources ($I_n\ n = 1, \ldots, N_{eq}$), uniformly distributed in the volume occupied by the EUT. Half wavelength is the optimal choice to space the equivalent sources [18]. These equivalent sources are small dipoles representing an electric current density distribution and small loops representing magnetic current density distribution. In both cases I_n represents their feeding current.
3. The impedance matrix Z_{ni} is calculated; each element represents the electric field at the position of the i-th monopole generated by the n-th equivalent source, fed by a unitary current. Expressions to determine analytically the impedance matrix are reported in Appendix.
4. The reference values of the electric field at the first iteration are set equal to the measured ones.

$$E_{i,k=0}^{ref} = E_i^{meas} \tag{1}$$

5. The iterative process starts here: at k-th iteration for each n-th equivalent source, the value of the feeding current (I_n) that best reconstructs the electric field over all the monopoles, is analytically determined by minimizing the normalized distance $d_{n,k}$,

$$d_{n,k} = \frac{\sum_{i=1}^{N_s} \left| E_{i,k}^{ref} - Z_{ni} I_n \right|}{\sum_{i=1}^{N_s} \left| E_i^{meas} \right|} \tag{2}$$

where E_i^{ref} represents the electric field to be reconstructed that is equal to E_i^{meas} in the first iteration of the algorithm, and it is equal to E_i^{meas} in the successive iterations, and $Z_{ni}I_n$ represents the electric field generated by I_n current at i-th monopole position.

6. The $n*$ equivalent source that gives the minimum $d_{n,k}$ is identified.

$$d_k = min(d_{n,k}) \quad \mathrm{n} = 1, \ldots, \mathrm{N}_{eq} \tag{3}$$

7. The $E_{i,k}^{ref}$ values of the electric field are updated with the new values that correspond to the residual field:

$$E_{i,k}^{ref} = E_{i,k-1}^{ref} - Z_{ni} I_{n*,k} \quad i = 1, \ldots, N_s \tag{4}$$

8. The algorithm iterates k times from step 5 until d_k is lower than a fixed threshold.
9. At the end of the iterations, an optimal subset of the N_{eq} equivalent sources is selected and assigned. These currents are placed in free space condition and the value of the electric field radiated at a specific distance over all the directions of the space is computed.
10. The maximum field value represents the value of the radiated emission, and it can be compared to the free space electric field limit ruled by standards.

This algorithm requires complex values of E_i^{meas} to provide an accurate prediction of free space radiated emission. Therefore, in the case of scalar field measurements, before applying the algorithm, a preliminary process is necessary. It consists in assigning a proper phase to the measured field samples.

In order to identify a suitable phase this procedure is applied:

- the first 6 steps of the algorithm, described above, are applied, finding the equivalent source ($I_{\mathrm{n}*,1}$) that, according to step 6, better approximate the measured electric field amplitudes.
- the complex field values produced by $I_{\mathrm{n}*,1}$ in all the N_s sample points are computed.
- The phases of these field values are assigned to each corresponding measured field amplitude, so we have complex values of E_i^{meas}.

At this point the algorithm restarts using these complex E_i^{meas} values.

The accuracy of this new procedure is lower than in the case we measure the complex values of the electric field samples, but its inaccuracy can be determined a priori, as shown in Section IV.

It must be highlighted that, the fact of assigning to the electric field samples the phase related to the equivalent source that best reconstruct the samples has two main reasons. Firstly, the first equivalent source represents the main

radiating behavior of the unintentional emissions of the EUT. As an example, in the case of common mode radiation due to a cable, an electric current parallel to the cable would better represent the nature of the radiation of the EUT. Secondly, the algorithm converges faster and to values closer to E_i^{meas}. If we assign to the electric field samples the phase equal to zero or the phase of other equivalent sources, it was numerically observed a worst behavior of the algorithm itself.

As regards computational time, the most burden operation is the computation of the impedance matrix Z_{ni}. It requires less than an hour (56'48" using a workstation equipped by two CPU Intel Xeon E5640 2.66GHz, 24GB of RAM and a GPU Nvidia Quadro FX1800 - 768MB).

The algorithm works in the frequency domain, so matrix Z_{ni} must be calculated for each considered frequency. However, this matrix does not change during the iterations of the algorithm, so, fixed the equivalent sources, it shall be calculated just once.

The iterations (points 4 to 7 of the algorithm) need much less time to be terminated. Using the same workstation, they last for approximately 90 seconds.

III. EXPERIMENTAL RESULTS

The experimental setup used to perform the measurements is illustrated in Figure 1.

The RC is a rectangular cavity having dimensions 800 mm × 900 mm × 1000 mm and it is made of galvanized steel. On each face of the RC there are 20 holes, irregularly positioned, for a total of 120 holes.

Three in-house EUTs were tested:

- A loop, having a radius of 6 cm [20].
- A slot over a metallic box; it has dimensions of 90 mm × 100 mm × 200 mm. In the wider face, a rectangular slot (75 mm × 2 mm) was opened and in the orthogonal face, an SMA pass-through connector was inserted to feed a folded monopole placed inside the box.
- The chassis of a power supply for a PC; it has dimensions of 85 mm × 120 mm × 150 mm; there are apertures on its faces, made for heating issue, and an irregular circuit was inserted inside of it to simulate a current path in a printed board.

More details of these EUTs can be found in [19].

The objective of this work is to describe the extension of the method proposed in [19], based on the complex values of the electric field samples, to the proposed one, where only the amplitude of the electric field samples is needed.

For this reason, in order to compare the accuracy of the two versions of the algorithm, we used the same measurement setup, and the same frequencies: 1, 2, and 3 GHz [19].

During the measurements, the EUT was placed inside the working volume of the RC and was fed using port 1 of a Vectorial Network Analyzer (VNA), through two coaxial cables and an N-type pass-through connector. The measuring monopole provided with a SMA female panel connector (length = 21 mm), was connected to port 2 of the VNA using another coaxial cable. The electric field was measured inserting sequentially the monopole in all the 120 holes made on the walls of the RC.

The strength of the electric field received by the monopole antenna in the n-th position is determined using equation (5)

$$E_n = abs\left(\sqrt{50 \cdot P_{VNA}}\,|S_{21}|\,\frac{50 + Z_{ant}}{50 \cdot l_{eff}}\right), \tag{5}$$

where P_{VNA} is the output power of the VNA, Z_{ant} and $\cdot l_{eff}$ are the impedance and the effective length of the monopole antenna respectively.

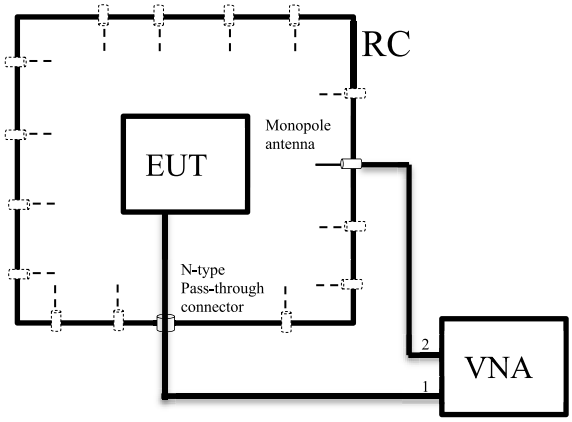

FIGURE 1. Measurement Setup.

FIGURE 2. The reverberation chamber (a), the monopole antenna (b), the loop (c), the metallic box with a slot (d) and the chassis of a power supply (e).

Using (4), we obtained the value of the amplitude of the electric field samples collected by monopole antenna, thus emulating the behavior of a scalar instrument as an EMI receiver or a spectrum analyzer.

The radiated emission was measured according to the proposed method described in the previous section, based on the knowledge of the amplitude of the electric field on the RC walls. These values were compared with reference emission retrieved for measurements in an anechoic environment (AE), and with the measurements in RC using the complex values version of our method. In the three scenarios the maximum electric field at a distance of 2.3 m from the EUT, over all the spatial directions represents the value of the radiated emissions. This distance is due to the measurement setup constraint in the AE environment used in our labs (more details can be found in [19]).

In both RC scenarios we consider three electric and three magnetic equivalent sources, placed in each point of a grid of $9 \times 9 \times 9$ points, for a total of 4374 equivalent sources, chosen according to criteria presented in [18].

Table 1 reports these results and their ratio in dB with respect to reference emission.

TABLE 1. Radiated emissions measurements.

EUT	Frequency [GHz]	AE (reference) [mV/m]	RC (complex values)		RC (amplitude only)	
			mV/m	RC/AE [dB]	mV/m	RC/AE [dB]
Loop	1	1.8	1.9	0.47	1.9	0.47
Loop	2	2.9	2.8	-0.30	3.1	0.58
Loop	3	5.3	5.6	0.48	4.9	-0.68
Slot	1	82.9	84.6	0.18	77.6	-0.57
Slot	2	74.6	77	0.28	87.2	1.35
Slot	3	32.9	36.1	0.81	26.7	-1.81
Power Supply	1	26.6	28.6	0.63	25	-0.54
Power Supply	2	32.9	33.8	0.24	32.4	-0.13
Power Supply	3	37.8	38.4	0.14	42.7	1.06

Radiated emission measurement: comparison between measurements performed in anechoic environment (reference values), and measurement in RC using both complex values of the electric field samples and their amplitude only.

Results indicate that even without the knowledge of the phase of the electric field samples, the reconstruction of the radiated emissions is accurate, with an inaccuracy lower than 2 dB.

IV. UNCERTAINTY DETERMINATION

The algorithm for the determination of the radiated emission in a Multiple Monopole Stirred RC is based on the knowledge of the values of the electric field collected by the antennas.

If we know the complex value of these samples, it has been demonstrated [17], [18], [19] that their reconstruction is very accurate and, after some hundreds of iterations, the algorithm finds the values of the currents feeding the equivalent sources that reconstruct the samples with a good level of accuracy (error lower than 1%).

When we know only the amplitude of the electric field, the reconstruction of the samples is less accurate; as an example, Fig. 3 shows the accuracy level parameter $(1 - d_k)$ for the loop described in the previous section at the frequency of 1 GHz, both when the reconstruction is done with the complex value of the field sample and with the amplitude only value.

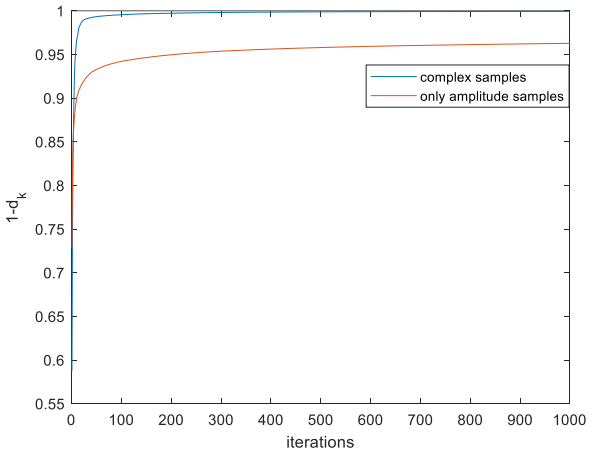

FIGURE 3. Accuracy on sample reconstruction for a 6 cm diameter loop at the frequency of 1 GHz.

It is possible to perform statistical analysis on how the inaccuracy of the reconstruction on the electric samples affects the determination of the radiated emission in free space conditions.

At this scope, combinations of the sources proposed in [16] were used to represent the radiating behavior of generic EUTs. These sources were simulated using the classical modal approach inside the cavity.

These sources are:

- Dipole(s) representing a dominant common mode radiation.
- Loop(s) representing a dominant differential mode radiation.
- Slot(s), in the case of aperture in the chassis of the device.
- Long monopole(s), in the case of feeding or communication cables.

The following procedure was adopted to perform the statistical analysis: using a Monte Carlo simulation, we varied the number, dimension, and position of the above-mentioned sources, so simulating different typologies of EUT.

Then we used the analytical algorithm described in [17] and [18] to get both the theoretical value (E^{ref}, reference values) of radiated emission of these sources and the

value of the radiated emission reconstructed (E^{rec}) from the electric samples evaluated on the walls of the RC, placed at the same positions of the holes present in the chamber.

Different values of E^{rec} were computed, each one corresponding to an interval of values of the indicator $(1 - d_n)$ from 0.7 to 0.95 with a step of 0.05.

Supplement 1 to the GUM (Guide to the expression of uncertainty in measurement) [21], [22], [23] suggests using formula (6) to propagate the uncertainty related to Monte Carlo simulations into a measurement uncertainty

$$u(x) = \sqrt{\frac{\nu_p}{\nu_p - 2}} \frac{\sigma_p}{\sqrt{n}}, \nu_p \geq 3 \tag{6}$$

where σ_p is the uncertainty related to Monte Carlo simulations, ν_p is their number, and $u(x)$ is the uncertainty related to n measurements.

In our scenario, we fixed $\nu_p = 100$ and $n = 1$; the choice to fix $\nu_p = 100$ is a good compromise between the significance of the simulations and the computing time; the last choice is common in EMI tests, usually performed only once for time and costs reasons.

Table 2 reports the results of the statistical analysis on a set of 100 simulations. In particular, it shows the ratio (in percentage) between the reconstructed and reference radiated emission level and the relative standard deviation evaluated according to (7):

$$\sigma_{dB} = 20log_{10}\left(\frac{\sigma + \mu}{\sigma}\right), \tag{7}$$

where σ and μ are the standard deviation and the mean value of the 100 maximum radiated emission values obtained with the reconstruction procedure.

Tables 2 shows that standard deviation, as expected, depends on parameter $(1 - d_k)$. Fixing this parameter, the standard deviations do not vary significantly among analyzed frequencies and devices.

TABLE 2. Radiated emissions accuracy.

Frequency [GHz]	$(1\text{-}d_k)$ [%]	(E^{rec}/E^{ref})[%]	σ_{dB}
1	70-75	79.0	1.71
1	75-80	84.9	1.49
1	80-85	86.0	1.24
1	85-90	89.9	0.97
1	90-95	93.0	0.98
1	95-100	97.4	0.60
2	70-75	82.3	1.96
2	75-80	80.7	1.73
2	80-85	81.2	1.49
2	85-90	83.1	1.30
2	90-95	86.9	1.15
2	95-100	95.5	0.81
3	70-75	82.2	2.15
3	75-80	76.7	2.00
3	80-85	83.5	1.73
3	85-90	87.2	1.40
3	90-95	88.8	0.93
3	95-100	95.6	0.73

Radiated emission accuracy: variance is a result of the statistical analysis on Monte Carlo simulations.

V. CONCLUSION

This paper concerns the extension of a method to reconstruct the maximum radiated emission of a device in a reverberation chamber equipped with multiple monopole source stirring technique by the knowledge of the strength of the electric field samples, collected by the monopole antennas mounted on the walls.

The proposed method is directly applicable in a classic radiated emission setup, where an EMI receiver or a spectrum analyzer is used.

Although the lack of information on the phase in measured data, the accuracy of the proposed method, evaluated through statistical analysis, is well acceptable.

Measurements confirm the usability of the method in all the explored frequency range.

The measurement time is about two hours, but at the current state of the art, the monopoles are manually inserted into the holes present in the walls of the RC. In the case of an electronic switch, measurement time will be certainly reduced.

To further decrease the measurement time, the possibility of reducing the number of electric samples by selecting a subset of the 120-hole positions will be investigated in the future, and, in particular, the effect of their reduction on the accuracy of reconstruction of the radiated emissions.

APPENDIX

The expression to be used for the evaluation of Z_{ni} depends on the orientation (r) of the n-th equivalent source and on the direction (s) of the i-th monopole on wall. Considering a cartesian coordinate system, nine combinations of orientations are possible.

Let's assume that the RC has dimension a along x direction, b along y direction and d along z direction.

Applying the classical modal approach, the possible Z_{ni} expression are easily to obtain.

Considering the element of electric current I_z having length l_d and oriented along the z axis, placed in (x_d, y_d, z_d), the electric field on the RC wall orthogonal to x axis, at the

position (y, z) is

$$E_x^{(z)(x)} = Z_{ni}^{(z)(x)} I_z = -\frac{16 I_z}{j\omega\varepsilon} \sum_{m,n,p} \left[\frac{1}{abd} \, sin\left(k_y y\right) \sin\left(k_z z\right) \cdot \right.$$
$$\cdot \sin(k_z l_d) \sin\left(k_x x_d\right) \sin\left(k_y y_d\right) \sin\left(k_z z_d\right) \cdot$$
$$\left. \cdot \left(\frac{k_x}{k_{nmp}^2} + \frac{k_x k^2}{\delta_p k_{nmp}^2 \left(k_{nmp}^2 - k_{TM}^2\right)} \right) \right], \tag{A-1}$$

where

$$k_x = \frac{m\pi}{a}, \quad k_y = \frac{n\pi}{b}, \; k_z \frac{p\pi}{d},$$
$$k_{mnp}^2 = k_x^2 + k_y^2 + k_z^2, k_c^2 = k_x^2 + k_y^2,$$
$$\delta_i = \begin{cases} 2, & i = 0 \\ 1, & i \neq 0, \end{cases}$$
$$k_{TE,TM}^2 = k^2 \left(1 - (j-1) \frac{\omega_{mnp}}{\omega Q_{mnp}^{TE,TM}} \right),$$

k is the wavenumber, ω_{mnp} is the angular resonant frequency for the (m, n,p)-th mode and $Q_{mnp}^{TE,TM}$ is the quality factor of the RC related to the (m,n, p)-th TE or TM mode.

Considering the element of electric current I_y having length l_d and oriented along the y axis, placed in (x_d, y_d, z_d), the electric field on the RC wall orthogonal to x axis, at the position (y, z) is

$$E_x^{(y)(x)} = Z_{ni}^{(y)(x)} I_y = -\frac{16 I_y}{j\omega\varepsilon} \sum_{m,n,p} \left[\frac{1}{abd} \, sin\left(k_y y\right) \sin\left(k_z z\right) \cdot \right.$$
$$\cdot \sin\left(k_y l_d\right) \sin\left(k_x x_d\right) \sin\left(k_y y_d\right) \sin\left(k_z z_d\right) \cdot$$
$$\cdot \left(\frac{k_x}{k_{nmp}^2} + \frac{k_x k^2}{\delta_m \delta_n k_c^2 \left(k_{nmp}^2 - k_{TE}^2\right)} \right.$$
$$\left. \left. - \frac{k_x k_z^2 k^2}{\delta_p k_{nmp}^2 k_c^2 \left(k_{nmp}^2 - k_{TM}^2\right)} \right) \right] \tag{A-2}$$

Considering the element of electric current I_x having length l_d and oriented along the x axis, placed in (x_d, y_d, z_d), the electric field on the RC wall orthogonal to x axis, at the position (y, z) is

$$E_x^{(x)(x)} = Z_{ni}^{(x)(x)} I_x = -\frac{16 I_x}{j\omega\varepsilon} \sum_{m,n,p} \left[\frac{1}{abd} \, sin\left(k_y y\right) \sin\left(k_z z\right) \cdot \right.$$
$$\cdot \sin\left(k_x l_d\right) \sin\left(k_x x_d\right) \sin\left(k_y y_d\right) \sin\left(k_z z_d\right) \cdot$$
$$\cdot \left(\frac{k_x}{k_{nmp}^2} + \frac{k_y^2 k^2}{\delta_m \delta_n k_x k_c^2 \left(k_{nmp}^2 - k_{TE}^2\right)} \right.$$
$$\left. \left. - \frac{k_x k_z^2 k^2}{\delta_p k_{nmp}^2 k_c^2 \left(k_{nmp}^2 - k_{TM}^2\right)} \right) \right] \tag{A-3}$$

Considering the element of electric current I_z having length l_d and oriented along the z axis, placed in (x_d, y_d, z_d), the electric field on the RC wall orthogonal to y axis, at the position (x, z) is

$$E_y^{(z)(y)} = Z_{ni}^{(z)(y)} I_z = -\frac{16 I_z}{j\omega\varepsilon} \sum_{m,n,p} \left[\frac{1}{abd} \, sin\left(k_x x\right) \sin\left(k_z z\right) \cdot \right.$$
$$\cdot \sin\left(k_z l_d\right) \sin\left(k_x x_d\right) \sin\left(k_y y_d\right) \sin\left(k_z z_d\right) \cdot$$
$$\left. \cdot \left(\frac{k_y}{k_{nmp}^2} - \frac{k_y k^2}{\delta_p k_{nmp}^2 \left(k_{nmp}^2 - k_{TM}^2\right)} \right) \right] \tag{A-4}$$

Considering the element of electric current I_y having length l_d and oriented along the y axis, placed in (x_d, y_d, z_d), the electric field on the RC wall orthogonal to y axis, at the position (x, z) is

$$E_y^{(y)(y)} = Z_{ni}^{(y)(y)} I_y = -\frac{16 I_y}{j\omega\varepsilon} \sum_{m,n,p} \left[\frac{1}{abd} \, sin\left(k_x x\right) \sin\left(k_z z\right) \cdot \right.$$
$$\cdot \sin\left(k_y l_d\right) \sin\left(k_x x_d\right) \sin\left(k_y y_d\right) \sin\left(k_z z_d\right) \cdot$$
$$\cdot \left(\frac{k_y}{k_{nmp}^2} - \frac{k_x^2 k^2}{\delta_m \delta_n k_y k_c^2 \left(k_{nmp}^2 - k_{TE}^2\right)} \right.$$
$$\left. \left. - \frac{k_y k_z^2 k^2}{\delta_p k_{nmp}^2 k_c^2 \left(k_{nmp}^2 - k_{TM}^2\right)} \right) \right] \tag{A-5}$$

Considering the element of electric current I_x having length l_d and oriented along the x axis, placed in (x_d, y_d, z_d), the electric field on the RC wall orthogonal to y axis, at the position (x, z) is

$$E_y^{(x)(y)} = Z_{ni}^{(x)(y)} I_x = -\frac{16 I_x}{j\omega\varepsilon} \sum_{m,n,p} \left[\frac{1}{abd} \, sin\left(k_x x\right) \sin\left(k_z z\right) \cdot \right.$$
$$\cdot \sin\left(k_x l_d\right) \sin\left(k_x x_d\right) \sin\left(k_y y_d\right) \sin\left(k_z z_d\right) \cdot$$
$$\cdot \left(\frac{k_y}{k_{nmp}^2} + \frac{k_y k^2}{\delta_m \delta_n k_c^2 \left(k_{nmp}^2 - k_{TE}^2\right)} \right.$$
$$\left. \left. - \frac{k_y k_z^2 k^2}{\delta_p k_{nmp}^2 k_c^2 \left(k_{nmp}^2 - k_{TM}^2\right)} \right) \right] \tag{A-6}$$

Considering the element of electric current I_z having length l_d and oriented along the z axis, placed in (x_d, y_d, z_d), the electric field on the RC wall orthogonal to z axis, at the position (x, z) is

$$E_z^{(z)(z)} = Z_{ni}^{(z)(z)} I_z = -\frac{16 I_z}{j\omega\varepsilon} \sum_{m,n,p} \left[\frac{1}{abd} \, sin\left(k_x x\right) \sin\left(k_z z\right) \cdot \right.$$
$$\cdot \sin\left(k_z l_d\right) \sin\left(k_x x_d\right) \sin\left(k_y y_d\right) \sin\left(k_z z_d\right) \cdot$$
$$\left. \cdot \left(\frac{k_z}{k_{nmp}^2} - \frac{k_c^2 k^2}{\delta_p k_z k_{nmp}^2 \left(k_{nmp}^2 - k_{TM}^2\right)} \right) \right] \tag{A-7}$$

Considering the element of electric current I_y having length l_d and oriented along the y axis, placed in (x_d, y_d, z_d), the electric field on a side the RC orthogonal to z axis, at the position (x, z) is

$$E_z^{(y)(z)} = Z_{ni}^{(y)(z)} I_y = -\frac{16 I_y}{j\omega\varepsilon} \sum_{m,n,p} \left[\frac{1}{abd} \, sin\,(k_x x) \sin\,(k_z z) \cdot \right.$$
$$\cdot \sin\,(k_x l_d) \sin\,(k_x x_d) \sin\left(k_y y_d\right) \sin\,(k_z z_d) \cdot$$
$$\left. \cdot \left(\frac{k_z}{k_{nmp}^2} + \frac{k_z k^2}{\delta_p k_z k_{nmp}^2 \left(k_{nmp}^2 - k_{TM}^2\right)} \right) \right] \qquad \text{(A-8)}$$

Considering the element of electric current I_x having length l_d and oriented along the x axis, placed in (x_d, y_d, z_d), the electric field on a side the RC orthogonal to z axis, at the position (x, z) is

$$E_z^{(x)(z)} = Z_{ni}^{(x)(z)} I_x = -\frac{16 I_x}{j\omega\varepsilon} \sum_{m,n,p} \left[\frac{1}{abd} \, sin\,(k_x x) \sin\,(k_z z) \cdot \right.$$
$$\cdot \sin\left(k_y l_d\right) \sin\,(k_x x_d) \sin\left(k_y y_d\right) \sin\,(k_z z_d) \cdot$$
$$\left. \cdot \left(\frac{\boldsymbol{k_z}}{\boldsymbol{k_{nmp}^2}} + \frac{\boldsymbol{k_z k^2}}{\boldsymbol{\delta_p k_z k_{nmp}^2 \left(k_{nmp}^2 - k_{TM}^2\right)}} \right) \right] \qquad \text{(A-9)}$$

These expressions were derived in starting from the general expression of a cavity field in terms of modal expansion [24].

REFERENCES

[1] European Standards (European Norms), "EN 55032 conducted and radiated EMI emissions," 2016.

[2] *Electromagnetic Compatibility (EMC)—Part 6–4: Generic Standards—Emission Standard for Industrial Environments*, document IEC 61000-6-4, International Electrotechnical Commission, Geneva, Switzerland, 2006.

[3] *Electromagnetic Compatibility (EMC)—Part 4: Testing and Measurement Techniques. Section 20: Emission and Immunity Testing in Transverse Electromagnetic (TEM) Waveguides. Committee Draft CISPR/A/278/CD*, document IEC 61000-4-20, International Electrotechnical Commission, Geneva, Switzerland, 2022.

[4] *Reverberation Chamber Test Methods*, International Electrotechnical Commission (IEC), Standard 61000-4-21, 2011.

[5] G. Koepke, D. Hill, and J. Ladbury, "Directivity of the test device in EMC measurements," in *Proc. IEEE Int. Symp. (EMC)*, Washington, DC, USA, Aug. 2000, pp. 535–539.

[6] P. F. Wilson, D. A. Hill, and C. L. Holloway, "On determining the maximum emissions from electrically large sources," *IEEE Trans. Electromagn. Compat.*, vol. 44, no. 1, pp. 79–86, Feb. 2002.

[7] P. Corona, G. Latmiral, E. Paolini, and L. Piccioli, "Use of a reverberating enclosure for measurements of radiated power in the microwave range," *IEEE Trans. Electromagn. Compat.*, vols. EMC–18, no. 2, pp. 54–59, May 1976.

[8] F. Leferink, J. C. Boudenot, and W. Van Etten, "Experimental results obtained in the vibrating intrinsic reverberation chamber," in *Proc. IEEE Int. Symp. Electromagn. Compat.*, Washington, DC, USA, Aug. 2000, pp. 639–644.

[9] D. Barakos and R. Serra, "Performance characterization of the oscillating wall stirrer," in *Proc. Int. Symp. Electromagn. Compat. (EMC)*, Angers, Sep. 2017, pp. 1–4.

[10] Y. Huang and D. J. Edwards, "A novel reverberating chamber: The source-stirred chamber," in *Proc. 8th Int. Conf. Electromagn. Compat.*, Edinburgh, U.K., Sep. 1992, pp. 120–124.

[11] R. Serra, A. C. Marvin, F. Moglie, V. M. Primiani, A. Cozza, L. R. Arnaut, Y. Huang, M. O. Hatfield, M. Klingler, and F. Leferink, "Reverberation chambers a La carte: An overview of the different mode-stirring techniques," *IEEE Electromagn. Compat. Mag.*, vol. 6, no. 1, pp. 63–78, 1st Quart., 2017.

[12] R. Serra, "Reverberation chambers through the magnifying glass: An overview and classification of performance indicators," *IEEE Electromagn. Compat. Mag.*, vol. 6, no. 2, pp. 76–88, Jul. 2017.

[13] A. De Leo, V. M. Primiani, P. Russo, and G. Cerri, "Low-frequency theoretical analysis of a source-stirred reverberation chamber," *IEEE Trans. Electromagn. Compat.*, vol. 59, no. 2, pp. 315–324, Apr. 2017.

[14] A. De Leo, G. Cerri, P. Russo, and V. Mariani Primiani, "Experimental comparison between source stirring and mechanical stirring in a reverberation chamber by analyzing the antenna transmission coefficient," in *Proc. Int. Symp. Electromagn. Compat. (EMC EUROPE)*, Aug. 2018, pp. 677–682.

[15] A. De Leo, V. M. Primiani, P. Russo, and G. Cerri, "Analytical prediction of common mode noise in a source stirred reverberation chamber," in *Proc. IEEE Int. Symp. Electromagn. Compat.*, Sep. 2015, pp. 1207–1212.

[16] L. A. De, G. Cerri, P. Russo, and V. M. Primiani, "Statistical analysis of the induced voltage on a DUT in a reverberation chamber where mechanical and source stirring actions are implemented," in *Proc. Int. Symp. Electromagn. Compat. (EMC EUROPE)*, Sep. 2019, pp. 241–246.

[17] A. De Leo, G. Cerri, P. Russo, and V. M. Primiani, "A novel emission test method for multiple monopole source stirred reverberation chambers," *IEEE Trans. Electromagn. Compat.*, vol. 62, no. 5, pp. 2334–2337, Oct. 2020.

[18] A. De Leo, G. Cerri, P. Russo, and V. M. Primiani, "A general method for radiated emission prediction in a multiple monopole source stirred reverberation chamber," *IET Sci., Meas. Technol.*, vol. 15, no. 7, pp. 588–596, Sep. 2021.

[19] A. De Leo, G. Cerri, P. Russo, and V. M. Primiani, "Experimental validation of an emission test method for source stirred reverberation chamber," *IEEE Trans. Electromagn. Compat.*, vol. 64, no. 1, pp. 11–18, Feb. 2022.

[20] *7405 E & H Near Field Probe Set*. Accessed: Nov. 2022. [Online]. Available: https://www.ets-lindgren.com/datasheet/probes-monitors/eh-near-field-probe-sets/9004/900401

[21] *Evaluation of Measurement Data—Supplement 1 to the 'Guide to the Expression of Uncertainty in Measurement'—Propagation of Distributions Using a Monte Carlo Method*, International Organization for Standardization, Geneva, Switzerland, 2008.

[22] C. F. M. Carobbi, "The GUM supplement 1 and the uncertainty evaluations of EMC measurements," in *Proc. IEEE-EMC Newslett.*, no. 225, Jun. 2010, pp. 53–57.

[23] C. F. M. Carobbi, M. Cati, and C. Panconi, "Note on the expected value and standard deviation of the mismatch correction," *IEEE Trans. Electromagn. Compat.*, vol. 53, no. 4, pp. 1098–1099, Nov. 2011.

[24] V. Bladel, *Electromagnetic Fields*, 2nd ed. Hoboken, NJ, USA: Wiley, 2007, pp. 509–562.

ALFREDO DE LEO (Member, IEEE) was born in Bari, Italy, in 1975. He received the Graduate degree (summa cum laude) in electronic engineering and the Ph.D. degree in electromagnetism and bioengineering from the University of Ancona, Italy, in 1999 and 2014, respectively. He is currently with the Antenna and EMC Laboratories, Università Politecnica delle Marche. His current research interests include the development of electromagnetic models, laboratory experiments and numerical simulation techniques related to interactions between electromagnetic fields and biological beings, and remote sensing of physiological activities and reverberation chambers. He is a member of the IEEE Electromagnetic Compatibility Society, the Italian Society of Electromagnetics (SIEM), and Consorzio Nazionale Interuniversitario per le Telecomunicazioni (CNIT). He is an Expert Member of IET TC 77/JMT MU Technical Committee No. 77: Electromagnetic Compatibility JMT MU: Measurement Uncertainty and CEI Technical Subcommittees SC210/7713 and SC 210/A.

PAOLA RUSSO (Member, IEEE) received the Ph.D. degree in electronic engineering from the Polytechnic of Bari, in April 1999. In 1999, she worked with a research contract at the Motorola Florida Research Laboratory, where she works on the analysis of an exposure system employed in a long-term study of RF exposure on mice. From 2000 to 2004, she worked with a research contract on the development of numerical tools applied to the coupling of electromagnetic field and biological tissue, and to different EMC problems. From January 2005 to July 2019, she worked as an Assistant Professor at the Università Politecnica delle Marche, where she has been appointed as an Associate Professor, since August 2020. She teaches antenna design and fundamental of electromagnetics. Her main research interests include the application of numerical modeling to EMC problem, antenna problem, plasma antennas, electromagnetic sensors. She is a SIEM Member.

VALTER MARIANI PRIMIANI (Senior Member, IEEE) received the Laurea degree (summa cum laude) in electronic engineering from the University of Ancona, Ancona, Italy, in 1990. He is currently an Associate Professor in electromagnetic compatibility (EMC) with Università Politecnica delle Marche, Ancona. He is currently a member with the Department of Information Engineering, where he is also responsible for the EMC Laboratory. His research interests include the prediction of digital printed circuit board radiation, the radiation from apertures, the electrostatic discharge coupling effects modeling, and the analysis of emission and immunity test methods. Since 2003, he has been involved in research activities on the application of reverberation chambers for compliance testing, metrology applications, and multipath propagation emulation. He has been a member of the COST Action 1407 ACCREDIT on the characterization of stochastic emissions from digital equipment. He is a Senior Member of the IEEE (EMC Society) and a member of the Italian Society of Electromagnetics. Since 2007, he has been an Active Member of some working groups for the development of IEEE Standards: 299.1, 1302, 2715, and 2716 on shielding effectiveness measurements. Since 2014, he has been a member of the International Steering Committee of EMC Europe. Since 2017, he has also been the Chair of the Working Group for the IEEE Standard P2718. He is currently an Associate Editor of the *IET Science, Measurement and Technology* journal.

Open Access funding provided by 'Università Politecnica delle Marche' within the CRUI CARE Agreement